



HAL
open science

A precise relationship among Buller's drop, ballistospore and gill morphologies enables maximum packing of spores within gilled mushrooms.

Martina Iapichino, Yen Wen Wang, Savannah Gentry, Anne Pringle, Agnese Seminara

► To cite this version:

Martina Iapichino, Yen Wen Wang, Savannah Gentry, Anne Pringle, Agnese Seminara. A precise relationship among Buller's drop, ballistospore and gill morphologies enables maximum packing of spores within gilled mushrooms.. 2020. hal-03011381

HAL Id: hal-03011381

<https://hal.science/hal-03011381>

Preprint submitted on 18 Nov 2020

HAL is a multi-disciplinary open access archive for the deposit and dissemination of scientific research documents, whether they are published or not. The documents may come from teaching and research institutions in France or abroad, or from public or private research centers.

L'archive ouverte pluridisciplinaire **HAL**, est destinée au dépôt et à la diffusion de documents scientifiques de niveau recherche, publiés ou non, émanant des établissements d'enseignement et de recherche français ou étrangers, des laboratoires publics ou privés.

1 **SHORT TITLE: Maximum spore packing within mushrooms**

2 **A precise relationship among Buller's drop, ballistospore, and gill morphologies**
3 **enables maximum packing of spores within gilled mushrooms**

4 Martina Iapichino¹, Yen Wen Wang², Savannah Gentry², Anne Pringle²,
5 Agnese Seminara¹

6 ¹*Institut de Physique de Nice UMR7010, CNRS and Université Côte d'Azur, Nice,*
7 *France;* ²Departments of Botany and Bacteriology, University of Wisconsin-Madison,
8 Madison, WI, USA

9
10 **ABSTRACT**

11 Basidiomycete fungi eject basidiospores using a surface tension catapult. A fluid
12 drop forms at the base of each spore and, after reaching a critical size, coalesces
13 with the spore and launches it from the gill surface. It has long been hypothesized
14 that basidiomycete fungi pack the maximum number of spores into a minimal
15 investment of biomass. Building on a nascent understanding of the physics
16 underpinning the surface tension catapult, we modeled a spore's trajectory away
17 from a basidium and demonstrated that, to achieve maximum packing, the size of
18 the fluid drop, the size of the spore, and the distance between gills must be finely
19 coordinated. To compare the model to data, we measured spore and gill
20 morphologies from wild mushrooms and compared measurements to the model.
21 The empirical data suggest that in order to pack the maximum number of spores
22 into the least amount of biomass, the size of Buller's drop should be smaller but
23 comparable to the spore size. Previously published data of Buller's drop and spore
24 sizes support our hypothesis and also suggest a linear scaling between spore

1
2
3
4
5
6
7
8
9
10
11
12
13
14
15
16
17
18
19
20
21
22
23
24
25 radius and Buller's drop radius. Morphological features of the surface tension
26 catapult appear tightly regulated to enable maximum packing of spores. If
27 mushrooms are maximally packed and Buller's drop radii scale linearly with
28 spore radii, we predict that intergill distance should be proportional to spore
29 radius to the power $3/2$.

30 Keywords: ballistospory; fungi; morphometrics ; biomechanics

31 INTRODUCTION

32 Molds, yeasts, and mushrooms are ubiquitous across Earth. Estimates of the number of
33 fungal species range from 1 to more than 5 million (Blackwell 2011), and fungi in
34 ecosystems function as decomposers, mutualists and pathogens. Emerging fungal
35 diseases endanger crops as well as wild plants and animals, threatening food security,
36 but fungal diseases also alter forest dynamics and contribute to the extinction of
37 animals. Losses cost millions of US dollars in damage (Pennisi 2010; Fisher et al 2012;
38 Kupferschmidt 2012).

39 Most fungal bodies (mycelia) are immobile, typically hidden within substrates.
40 Fungi use spores to reproduce and travel away from a natal habitat. Spores are carried in
41 air currents away from a source and when a spore lands in a favorable environment, it
42 germinates and begins or extends the life cycle. Basidiomycota are among the most
43 common fungi, encompassing pathogens like the honey mushroom as well as
44 charismatic mushrooms like matsutake and the fly agaric. The phylum is defined by the
45 production of sexually derived spores (basidiospores) on a basidium. Basidiospores are
46 launched via a surface tension catapult. Among species of mushroom-forming fungi,
47 e.g. agarics and boletes, spores typically form in groups of four from basidia arranged
48 along the gills or pores of a mushroom, each spore attached to a sterigma. A drop of

1
2
3
4
5
6
7
8
9
10
11
12
13
14
15
16
17
18
19
20
21
22
23
24
25
26
27
28
29
30
31
32
33
34
35
36
37
38
39
40
41
42
43
44
45
46
47
48
49 liquid, known as Buller's drop, forms extracellularly at the base of each spore when
50 water condenses on the hilar appendix of a spore. Buller's drop then collapses onto
51 another adaxial drop formed along the longitudinal axis of the spore itself (FIG. 1).
52 Upon coalescence, surface energy is converted into kinetic energy. The spore is ejected
53 horizontally away from the basidium and sterigma. The spore decelerates to rest after a
54 few milliseconds and then falls vertically between two gills or within the pore.

55 Ballistospore discharge was first observed by Schmitz (1843). In the 20th
56 century, Buller (1909) described the phenomenon in more detail, observing the
57 discharge of the spore and describing both the formation of the drop at the hilar
58 appendix and the subsequent launch of the spore together with the drop. The drop is
59 now referred to as "Buller's drop" and the discharge understood as a "surface tension
60 catapult". We also use the phrase "spore-drop complex" to mean the entire spore
61 discharge complex, including the adaxial drop, Buller's drop and the spore. Progress in
62 understanding the anatomy and physics of the surface tension catapult was enabled by
63 the development of cameras. Webster et al. (1984) provided photographic evidence of
64 Buller's drop forming at the hilar appendix just before discharge and proposed a two-
65 phase mechanism for spore ejection: the first phase involved Buller's drop enveloping
66 the spore surface, acquiring momentum; the second entailed the sharing of momentum
67 and movement of the center of mass of the spore-drop complex, a result of rapid
68 wetting. Subsequent works modeled the conversion of surface energy into kinetic
69 energy with different degrees of complexity and imaged ballistospore launch with
70 progressively faster cameras (Pringle et al 2005; Noblin et al 2009; Stolze-Rybczynski
71 et al 2009; Fischer et al 2010b; Liu et al 2017). Pringle et al. (2005) observed
72 coalescence while Noblin et al. (2009) described the process as encompassing four
73 stages and estimated approximately half of the total surface energy was dissipated

1
2
3
4
5
6
7
8
9
10
11
12
13
14
15
16
17
18
19
20
21
22
23
24
25
26
27
28
29
30
31
32
33
34
35
36
37
38
39
40
41
42
43
44
45
46
47
48
49
50
51
52
53
54
55
56
57
58
59
60
61
62
63
64
65

74 during launch. Recently, Liu et al. (2017) moved beyond considerations of energy
75 balance to generate simulations of the fluid dynamics within the Buller's drop and the
76 adaxial drop during coalescence and described experiments with biomimetic drops.
77 These authors found that coalescence occurs in a regime where viscous dissipation in
78 the Buller's drop is negligible. Hence, energy is not dissipated to set Buller's drop in
79 motion, instead, it may be dissipated to break the spore from the sterigma. In addition,
80 Liu et al. (2017) found that the phenomenon known in physics as “pinning” of the
81 contact line (de Gennes 1985) provides directionality for the spore-drop complex as it
82 ejects away from the originating gill.

83 It has long been hypothesized that mushrooms form gills to increase the surface
84 area for spore production and pack the maximum number of spores into a minimal
85 investment of biomass (Buller 1909; McKnight and Roundy 1991; Fischer and Money
86 2010). To achieve an optimal morphology, the size of Buller's drop, the size of the
87 spore, and the distance between gills must be finely coordinated. While spore size and
88 intergill distance may be under genetic control (Kues and Liu 2000), Buller's drop forms
89 extracellularly (Webster et al 1989). Whether and how fungi control the size of Buller's
90 drop remains unknown, although data reporting characteristic sizes of Buller's drop for
91 different species suggest individual species do control size (Pringle et al 2005; Stolze-
92 Rybczynski 2009; Stolze-Rybczynski et al 2009; Fischer et al 2010b).

93 To explore whether the morphologies of gilled mushrooms enable the maximum
94 packing of spores within tissues, we first revisit the theory relating ejection velocity and
95 flight time to the horizontal distance travelled by a spore from the moment of launch to
96 the moment it begins settling underneath the gills (Buller 1909; Pringle et al 2005;
97 Noblin et al 2009; Stolze-Rybczynski et al 2009; Fischer et al 2010b; Liu et al 2017).
98 Using energy balance we obtain the ejection speed and highlight its dependence on the

1
2
3
4
5
6
7
8
9
10
11
12
13
14
15
16
17
18
19
20
21
22
23
24
25
26
27
28
29
30
31
32
33
34
35
36
37
38
39
40
41
42
43
44
45
46
47
48
49
50
51
52
53
54
55
56
57
58
59
60
61
62
63
64
65

99 sizes and densities of the spore and Buller's drop. Combining expressions for ejection
100 speed and flight time, we predict the distance travelled ballistically by the spore-drop
101 complex before downward sedimentation starts. We then use our model to elucidate the
102 criteria enabling maximum packing of spores. In the phase space made up of the three
103 variables *(i)* drop radius, *(ii)* spore radius (defined as the radius of a sphere with the
104 same volume as the spore) and *(iii)* intergill distance, the criterion for maximum
105 packing is that spores must travel ballistically exactly midway between two facing gills.
106 Given two of the three variables *(i)*-*(iii)*, the model predicts the third, assuming
107 maximum packing. To compare our model to empirical data, we collected mushrooms
108 of eight different species and measured spore size and intergill distance. By placing
109 these morphological data on the phase space generated from our model, we predict that
110 for collected species, the radius of Buller's drop that maximizes spore packing ranges
111 between 23% and 50% of the radius of the spore (depending on the precise value of
112 spore density and efficiency of energy conversion). To validate the prediction, we
113 revisit previously published data for an additional 13 species (Pringle et al 2005; Stolze-
114 Rybczynski 2009; Stolze-Rybczynski et al 2009; Fischer et al. 2010b) and find Buller's
115 drop scales as 32% of spore size, consistent with our prediction. These results suggest
116 that Buller's drop radius scales linearly with spore radius, and combined with our
117 model, generate a second prediction: to enable maximum packing, intergill distance
118 should be proportional to spore radius to the power 3/2. In the aggregate our work
119 synthesizes thinking about the morphologies of Buller's drop, spores, and gills, while
120 providing insights into the principles shaping ballistospory.

121 MATERIALS AND METHODS

122 *Spore ejection speed.*—The reduction in surface energy following coalescence is
123 $\sim\pi\gamma R_B^2$ where γ is surface tension of Buller's drop and R_B is Buller's drop radius. By

124 balancing surface energy to kinetic energy of the spore-drop complex $1/2(m_s +$
 125 $m_B)v_0^2$, we obtained:

$$126 \quad v_0 = \sqrt{\frac{2\pi\gamma\alpha R_B^2}{m_s + m_B}} \quad (1)$$

127 where v_0 is the ejection velocity and m_s and m_B are the mass of the spore and of
 128 Buller's drop. Note that we have neglected viscous dissipation because ballistospory
 129 operates in a regime of low Ohnesorge number (Liu et al 2017). By simple algebra we
 130 can express v_0 in the following form $v_0 = U \sqrt{\frac{y^2}{y^3 + \beta}}$ where $U = \sqrt{3\alpha\gamma/(2\rho_B R_S)}$ is a
 131 velocity scale independent of Buller's drop radius; R_S is the radius of a sphere with the
 132 same volume as the spore, this is the "equivalent radius" of the spore, and we will call it
 133 "spore radius" for short; $y = R_B/R_S$ is the normalized Buller's drop radius, i.e. the ratio
 134 of Buller's drop to spore radii; ρ_B and ρ_s are densities of Buller's drop and spore
 135 respectively and $\beta = \rho_s/\rho_B$ is the ratio of Buller's drop to spore densities. The
 136 parameter α accounts for the fraction of available energy dissipated when the spore
 137 breaks apart from the hilum, the point of attachment between the spore and the sterigma
 138 (FIG. 1).

139 ***Relaxation time of the spore-drop complex.***—The complex's relaxation time is
 140 determined by the air drag that causes rapid deceleration and is well approximated by
 141 the Stokes time (Stokes 1851; Fischer et al 2010a):

$$142 \quad \tau = \frac{2R^2}{9\bar{\beta}\nu} \quad (2)$$

143 where ρ_a , ρ_s and ρ_B are the densities of the air, of the spore and of Buller's drop
 144 respectively; $\bar{\beta} = \rho_a(R_S^3 + R_B^3)/(\rho_s R_S^3 + \rho_B R_B^3)$ is the density of air divided by the
 145 density of the spore-drop complex; ν is the kinematic viscosity of air and R is the radius
 146 of the spore-drop complex, which we consider as a sphere with volume equal to the sum

1 147 of the spore and drop volumes $R = (R_B^3 + R_s^3)^{\frac{1}{3}}$. When Buller's drop is considerably
2
3 148 smaller than the spore which is often the case, $\bar{\beta} \sim \rho_a / \rho_s$. Following simple algebra we
4
5 149 obtain the Stokes time of the spore-drop complex in the following non-dimensional
6
7
8 150 form $\tau = T(y^3 + 1)^{\frac{2}{3}}$ where $T = \frac{2R_s^2}{9\nu\bar{\beta}}$, ν is the air kinematic.

11
12
13 151 ***Data collection and published data.***—Between 15–17 Sep 2017 we collected
14
15 152 mushrooms from the Upper Peninsula of Michigan. On 15 Oct 2017 we collected
16
17 153 mushrooms from the University of Wisconsin-Madison Lakeshore Natural
18
19 154 Preserve. We collected opportunistically, taking any mushroom that appeared in
20
21 155 good shape, but focusing on gilled (not pored) fungi. We collected specimens of
22
23 156 eight morphologically distinct species (TABLE 2).

24
25
26
27 157 We also retrieved published data from the literature; these data were generated
28
29 158 from a different group of species (TABLE 3) and provide measurements of Buller's
30
31 159 drops and spores, but do not provide information about intergill distances (Pringle et al
32
33 160 2005; Stolze-Rybczynski 2009; Stolze-Rybczynski et al 2009; Fischer et al 2010b). In
34
35 161 this series of papers, the authors captured ballistospory from high speed video
36
37 162 microscopy and obtained Buller's drop and spore size (but not intergill distance) from
38
39 163 image analysis. We discarded the species for which measures of Buller's drop size was
40
41 164 inferred indirectly. When spore volume was available, spore radius was calculated as
42
43 165 $R_s = (\frac{3V_s}{4\pi})^{1/3}$. When spore volume was not available directly, we calculated it from
44
45 166 spore length and width, assuming spores are prolate spheroids, $V_s = \frac{4}{3}\pi L_s W_s^2$. Values of
46
47 167 spore densities range from 0.8 to 3.8 g/cm^3 (Hussein et al 2013).

48
49
50
51 168 Data from the literature were used to estimate the efficiency parameter α as
52
53 169 follows. For two species of basidiomycota (*Auricularia* and *Sporobolomyces*), for
54
55
56
57
58
59
60
61
62
63
64
65

170 which geometry of the spore and drop was observed directly, velocity of ejection was
171 73% and 68% of the theoretical maximum (Noblin et al. 2009), yielding a fraction of
172 usable energy $0.73^2 = 0.53$ and $0.68^2 = 0.46$, hence $\alpha = (50 \pm 5)\%$, consistent with
173 estimates presented in (Stolze-Rybczynski 2009), based on a different hypothesis about
174 the geometry of the adaxial drop.

175 ***Preparing specimens for morphometrics.***—On the same day mushrooms were
176 collected, a scalpel was used to separate caps from stems (FIG. 2A). Caps were left face
177 down for 8 to 12 hr on a piece of paper covered with aluminum foil in order to create
178 spore prints (FIG. 2B). Spore prints are generated when spores fall from gills and settle
179 directly underneath the cap. Spore prints reflect the morphology of each collected
180 specimen, and the location of stems and patterns of gill spacing are easily seen from a
181 spore print. To image spores, three small pieces of foil, each measuring approximately 1
182 mm \times 1 mm, were cut (i) from close to each stem, (ii) equidistant between the stem and
183 the cap edge, and (iii) from near the edge of each cap. Spores were washed off each foil
184 piece and suspended in a 0.01%vol solution of Tween 80. 15 μ L of each spore
185 suspension were immediately spread onto a glass slide and spores imaged. Microscope
186 slides were sealed with nail polish to minimize evaporation of the Tween solution and
187 prevent the movement of spores during imaging. To measure distances between gills, a
188 photograph of each cap's underside, with a ruler included in the photograph, was taken
189 immediately after spore printing using a Canon EOS400D.

190 ***Identification of species using DNA barcoding.***— Tentative field identifications were
191 confirmed by sequencing the nuc rDNA ITS1-5.8S-ITS region (ITS barcode; Schoch et
192 al. 2012) of each mushroom. To generate DNA barcodes for each collected mushroom,
193 we extracted DNA with an NaOH extraction method modified from Wang et al (1993).
194 First, the tissues of each sporocarp were ground finely with a pestle in 40 μ L of 0.5 M

195 NaOH and the solution centrifuged at 13 000 rpm for 10 min. 5 μ L of supernatant were
196 transferred to 495 μ L of 100 mM Tris-HCl (pH 8) and centrifuged at 13 000 rpm for
197 another min. Next, the resulting supernatant was used as template for PCR. We
198 amplified the ITS using primers ITS1F (Gardes and Bruns 1993) and ITS4 (White et al.
199 1990) following PCR protocols outlined in White et al. (1990) modified for Lucigen's
200 EconoTaq Plus Green 2x Master Mix (Lucigen Corp., Middleton, Wisconsin).
201 Amplified products were cleaned and then Sanger sequenced by Functional Biosciences
202 (Madison, Wisconsin). Sequences were deposited in GenBank under accession numbers
203 MK829236-MK829244. Two specimens, one *Mycena* (MK829242) and one *Russula*
204 (MK829243), could not be confidently identified to species despite their barcode data.

205 ***Microscopy and image analysis to measure spore geometry.***—

206 Images of spores were taken using microscopes housed at the Newcomb Image Center
207 at the University of Wisconsin-Madison. Spores were imaged either individually or in
208 groups (FIG. 2C), depending on whether a particular microscope's field of view housed
209 one or more than one spore, using Zeiss Elyra LSM 780 and Zeiss LSM 710 confocal
210 microscopes. Spores were not stained as all collected species proved to be
211 autofluorescent. The laser wavelength used to excite autofluorescence was 405 nm. The
212 average area S and average radius of spores $R_s = \sqrt{S/\pi}$ of each species were then
213 calculated from images of between 155–1180 spores using an image analysis tool
214 implemented in ImageJ v.1.51. A single pixel's dimension in μ m was calculated from
215 the microscope and the images converted to greyscale (8-bit or 16-bit). ImageJ was then
216 used to threshold each image and convert the greyscale to a binary image, highlighting
217 all the spores to be counted and using the measurement of a single pixel to calculate the
218 area of each spore as shown in FIG. 2C-D. Spores touching other spores were not

1
2
3
4
5
6 219 measured, nor were particles smaller than $2 \mu\text{m}^2$. Particles bigger than $2 \mu\text{m}^2$ were
7
8 220 identified either as spores or not by eye.
9
10 221 ***Image analysis to measure intergill distances.***—To measure distances between gills,
11 222 we first identified the center of each cap by eye (FIG. 2E). We then drew between 6 and
12 223 10 circles (depending on the size of each specimen's cap) concentrically around the
13 224 center of the cap (FIG. 2E). We then used ImageJ v1.51 to open each picture, set pixel
14 225 length in mm using the image of the ruler included in each photograph, and convert
15 226 images to greyscale (8-bit or 16-bit). The Oval Profile plugin was used to obtain
16 227 greyscale profiles traced along each of the concentric circles drawn onto an image.
17 228 Profiles were sampled at 3600 equally spaced points along each circle. Next, the area of
18 229 each circle was measured to calculate its average distance from the cap center, and these
19 230 measurements were later used to convert the distance between gills from radians to
20 231 mm. The greyscale profile obtained from ImageJ along each circle was imported into
21 232 Matlab R2017b (one example in FIG. 2F) and analyzed with the function Findpeaks.
22 233 Peaks in the greyscale image identify the centers of gills, which appear white in
23 234 greyscale images. Peaks that were closer than 0.3° were discarded as noise. We visually
24 235 inspected data to confirm that minor peaks did correspond to gills. Finally, we
25 236 quantified gill thickness as the width of the peak, defined as the distance where grey
26 237 value drops half way below peak prominence, which is a measure of peak height. The
27 238 distance between two gills, d , was defined as the distance between their centers minus
28 239 the half-width of each of the two gills (see close up of two peaks in FIG. 2G).

29
30
31
32
33
34
35
36
37
38
39
40
41
42
43
44
45
46
47
48
49
50
51
52
53
54
55
56 240

241 **RESULTS**

57
58
59 242 ***Ejection speed.***—We first focused on the velocity achieved by the surface tension
60
61
62
63
64
65

1
2
3
4
5
6
7
8
9
10
11
12
13
14
15
16
17
18
19
20
21
22
23
24
25
26
27
28
29
30
31
32
33
34
35
36
37
38
39
40
41
42
43
44
45
46
47
48
49
50
51
52
53
54
55
56
57
58
59
60
61
62
63
64
65

243 catapult, which depends on various physical parameters as well as on the dimensions of
244 the spore and Buller's drop. Let us first recapitulate the physical processes that lead to
245 spore launch. Buller's drop coalesces with the adaxial drop to power the surface tension
246 catapult; both drops are made from condensed water vapor and appear following the
247 secretion of hygroscopic substances by the fungus. When Buller's drop coalesces with
248 the adaxial drop, the resulting reduction of surface area provides the surface energy to
249 accelerate the spore. Because the adaxial drop is pinned to the surface of the spore,
250 Buller's drop accelerates along the axis of the spore towards its distal tip. Once the
251 moving drop reaches the tip of the spore, capillarity and contact line pinning decelerate
252 water, and its momentum is transferred to the spore. Momentum transfer causes the
253 force that breaks the contact between spore and sterigma, resulting in spore ejection
254 away from the basidium.

255 In this physical process, surface energy is converted in kinetic energy and by
256 using the physical principle of energy conservation we obtained equation (1)
257 (MATERIALS and METHODS): this equation predicts there will be a radius of Buller's
258 drop that maximizes v_0 (FIG. 3A). By zeroing the derivative in (1) we obtained the size
259 of Buller's drop that maximizes ejection speed: $y_{max} = (2\beta)^{1/3}$ and when considering
260 spores with densities once to twice the density of water (Hussein et al 2013), $\beta = 1$ to 2,
261 this equation implied that at y_{max} Buller's drop radius is comparable to the equivalent
262 radius of the spore $R_B \sim 1.26R_s$ to $1.59R_s$ (the gray shade in FIG. 3A marks all values of
263 y_{max} , for β ranging from 1 to 2). Note that at y_{max} control of the ejection speed is
264 robust, i.e. ejection speed becomes insensitive to small deviations from the exact value
265 of Buller's drop size. Buller's drop is generally assumed to scale with spore length
266 (Fischer et al. 2010b), and this scaling appears to hold for at least 13 species of
267 basidiomycetes, as shown in Pringle et al. (2005), Stolze-Rybczynski (2009), Stolze-

1
2
3
4
5
6
7
8
9
10
11
12
13
14
15
16
17
18
19
20
21
22
23
24
25
26
27
28
29
30
31
32
33
34
35
36
37
38
39
40
41
42
43
44
45
46
47
48
49
50
51
52
53
54
55
56
57
58
59
60
61
62
63
64
65

268 Rybczynski et al. (2009), and Fischer et al. (2010b). FIG. 3B uses these published data
269 to calculate spore radius R_s pointing to $y_{literature} = R_B/R_s \sim 0.32 \pm 0.08$ where we
270 report the best fit through the data and \pm the mean residual. $y_{literature}$ are represented
271 in cyan on the horizontal axis in FIG. 3A. Note that only three out of their 13 species
272 were gilled mushrooms (TABLE 3), but these three species lined up with the rest of the
273 data and showed no clear departure from the rest of the collected data (FIG. 3B).

274 **Ballistic range.**—In order to understand how far a spore-drop complex travels after
275 launch, we analyzed the timescale τ over which the spore-drop complex decelerates to
276 rest, or relaxation time (see MATERIALS AND METHODS). We found that after
277 discharge, spores travel horizontally a distance

$$278 \quad x = v_0 \tau$$

279 with v_0 and τ from equations (1) and (2). Next, a spore stops abruptly and starts
280 to sediment vertically, out from beneath a pair of facing gills, following a trajectory
281 commonly known as a "sporabola" (FIG. 4A).

282 **Maximum spore packing.**—In order to successfully escape the mushroom, a spore must
283 travel away from its basidium a distance x into the clear space between gills before
284 settling downwards; it must travel far enough to avoid entrapment within the basidia
285 and spores underneath it. If x is in fact dictated by this criterion that ensures spores
286 escape the gills without sticking to tissue underneath, and assuming all gills are
287 reproductive, then the distance between two facing gills, d , should be at least twice x ,
288 hence $d > 2x$. To pack as many spores as possible within a mushroom and avoid
289 inefficient empty spaces, the distance between gills must be close to this minimum
290 value:

$$291 \quad d = 2x$$

292 where $x = v_0\tau$. Maximum packing was first suggested by Buller (1909), and
 293 this relationship appeared explicitly in more recent literature (Stolze-Rybczynski et al.
 294 2009). Plugging in the values of v_0 and τ given by equations (1) and (2) we obtain:

295

$$297 \left(\frac{y_{pack}^2}{y_{pack}^3 + \beta} \right)^{1/2} (y_{pack}^3 + 1)^{2/3} = \frac{d}{2UT}$$

296

(3)

298 where U and T are the velocity and time scales derived in the previous two paragraphs
 299 and summarized in TABLE 1 and y_{pack} is the normalized Buller's drop radius, we add
 300 the suffix $_{pack}$ to stress that this prediction is valid at maximum packing. Equation (3)
 301 predicts the relationship between three variables: nondimensional Buller's drop radius
 302 y_{pack} , spore radius R_s (R_s is contained in the expressions for U and T summarized in
 303 TABLE 1) and intergill distance d - at maximum packing. Hence *given two of these*
 304 *three variables, equation (3) predicts the third*, assuming maximum packing and given
 305 the values of the parameters (spore density, energy conversion efficiency). For example,
 306 for any combination of spore radius and intergill distance, equation (3) predicts the
 307 optimal radius of Buller's drop that achieves maximum packing. We solve Equation (3)
 308 numerically and show the result for the normalized radius of Buller's drop, y_{pack} , in
 309 FIG. 4 color-coded from 0 (cyan) to 5 (black) for different combinations of intergill
 310 distances and spore radii using parameters listed in TABLE 1. At each point in the
 311 phase space defined by spore radius and intergill distance, the color represents the value
 312 of normalized Buller's drop radius that achieves maximum packing. Symbols and error
 313 bars represent our own data, described, analysed, and discussed below.

1
2
3
4
5
6
7
8
9
10
11
12
13
14
15
16
17
18
19
20
21
22
23
24
25
26
27
28
29
30
31
32
33
34
35
36
37
38
39
40
41
42
43
44
45
46
47
48
49
50
51
52
53
54
55
56
57
58
59
60
61
62
63
64
65

314 **Data collection.**— To compare our model to data, we measured spore and gill
315 morphologies (see MATERIALS and METHODS) for eight wild mushroom species
316 (TABLE 2). While spore size varied from species to species, spores within a single
317 mushroom cap were considerably more similar and there were no consistent pattern of
318 variation, e.g. spores were not larger nearer the center or edge of a cap) (FIG. 5).
319 Moreover, the average intergill distance also remains constant with distance from the
320 center of the cap. The phenomenon is driven by the appearance of secondary gills
321 (lamellulae) towards the edge of a mushroom cap; as two gills with origins at the stipe
322 diverge, often a secondary gill will appear. The appearance of secondary and tertiary
323 gills keeps intergill distances constant. The only species in our dataset with variable
324 intergill distances was an unidentified species of *Russula*, which did not produce
325 secondary gills (Phillips 1991; Fischer and Money 2010). Among measured species,
326 intergill distances varied from about 0.25 mm to 1.5 mm (FIG. 6), but there was no
327 obvious correlation between intergill distances and the size of the mushroom cap.

328 **To ensure maximum packing in real species, we predicted Buller's drop radius**
329 **should be 23% to 50% of spore radius.**—Here we used equation (3) and data about
330 spore radius and intergill distance to predict Buller's drop radius at maximum packing.
331 We computed average and standard deviation of spore radius and intergill distance
332 across single individuals and placed these data on the phase space generated by our
333 hypothesis for maximum spore packing (symbols and error bars in FIG. 4B). While
334 most parameters of our model are known (TABLE 1), α and ρ_s are not. In order to
335 understand how the model depended on parameters, we derived an approximate formula
336 from equation (3), showing that in our model the optimal radius of Buller's drop
337 depended only weakly on these free parameters. Indeed, when $y_{pack} < 1$, we could

338 expand equation (3) to leading order, i.e. neglecting the smallest terms in the equation.

339 In equation (3) we neglected $y_{pack}^3 \ll 1$ and $y_{pack}^3 \ll \beta$, to obtain:

$$340 \quad R_B \sim d \sqrt{\frac{27\rho_a v^2 \rho_a}{8\alpha\rho_s R_s \gamma}} \quad (4)$$

341 This compact formula explicitly connected the radius of Buller's drop at maximum
342 packing with the parameters of the problem. Particularly, it showed that Buller's drop
343 radius at maximum packing depended on $(\alpha\rho_s)^{-1/2}$. For the range of variation reported
344 in the literature (see TABLE 1), $\alpha\rho_s = 0.4 \text{ g/cm}^3$ to 1.9 g/cm^3 , and plugging these
345 values as well as data collected in this study in our model, we predicted that at
346 maximum packing $\langle y_{this\ study} \rangle = 50\%$ to 23% . Importantly, the observed value of y
347 from the literature is within this range of variation: $\langle y_{literature} \rangle \sim 32\%$, which supports
348 the hypothesis of maximum packing. The value of the fitting parameters for which the
349 predicted Buller's drop radius for maximum packing averaged over our collected data
350 fits the observed value, $\langle y_{this\ study} \rangle = \langle y_{literature} \rangle = 32\%$ is $\alpha\rho_s = 0.9 \text{ g/cm}^3$. For
351 the eight species analyzed in this study, we found a standard deviation of 12%. A
352 dataset of Buller's drop radius, spore radius, and intergill distance measured on the
353 same specimen is needed to further confirm the hypothesis of maximum packing.

354 ***Scaling of Buller's drop radius with intergill distance.***—Buller's drop is often
355 assumed to scale *proportionally* with spore size (Fischer et al. 2010b), and published
356 data shown in FIG. 3B corroborated this assumption (although note that only three out
357 of 13 species in these published data correspond to gilled mushrooms). However, the
358 assumption appears at odds with the prediction for maximum packing because equation
359 (4) implies that Buller's drop radius scales linearly with intergill distance d and with the
360 *inverse* square root of spore radius R_s . To resolve the paradox, intergill distance must
361 increase with increasing spore radius in the following way:

1
2
3
4
5
6
7
8
9
10
11
12
13
14
15
16
17
18
19
20
21
22
23
24
25
26
27
28
29
30
31
32
33
34
35
36
37
38
39
40
41
42
43
44
45
46
47
48
49
50
51
52
53
54
55
56
57
58
59
60
61
62
63
64
65

$$d \sim 0.32 \sqrt{\frac{8\gamma\alpha\rho_s}{27\rho_a^2 v^2}} R_s^3$$

365
362
363
364
366
367
368
369
370
371
372
373
374
375
376
377
378
379
380
381
382
383
384

where we have simply plugged $R_B \sim 0.32R_s$ into equation (4). In order to convincingly prove or disprove this relationship, further data monitoring spore, drop, and gill morphologies, as well as spore density and ejection velocity, are needed.

DISCUSSION

The intricate morphologies of gilled mushrooms are hypothesized to maximize surface to volume ratios, an adaptation enabling the maximum packing of spores within a minimal investment of biomass. The hypothesis requires intergill distances to be exactly twice the horizontal range of an ejected spore: an ejected spore must both clear its natal gill and avoid lodging into the gill across from it, and assuming gills are crowded together as closely as possible (to efficiently use the space within a mushroom cap), the spore will be finely tuned to reach midway between facing gills. Intergill distances may be shaped by the reach of a spore, but because spore range is dictated by the dimension of Buller's drop and its density relative to the dimension and density of the spore, the three parameters – intergill distance, spore size, and Buller's drop size – emerge as highly interdependent in the context of maximum packing. We find that intergill distances and spore sizes from empirical observations populate a region of phase space where our model predicts the radius of Buller's drop enabling maximum spore packing ranges from 23% to 50% of spore radius. Previously published data (Pringle et al 2005; Stolze-Rybczynski 2009; Stolze-Rybczynski et al. 2009; Fischer et al. 2010b) suggest Buller's drop radius scales with spore dimensions as $R_B \sim 32\% R_s$ and support the hypothesis of maximum packing. A further prediction of our model is

1
2
3 385 that the linear scaling of Buller's drop and spore radii implies intergill distance must
4
5 386 scale as $R_s^{3/2}$ within an optimally packed mushroom.

6
7 387 The fungi used in our analyses (FIG. 3A) do not operate at maximum ejection
8
9 388 speed; the velocity of ejection for these spores remains well below the maximum.
10
11 389 Whether other species operate at maximum ejection speed remains to be elucidated.
12
13 390 This result may not be surprising because robust control of ejection speed may not
14
15 391 contribute an obvious selective advantage. By contrast, the maximum packing of spores
16
17 392 is expected to contribute significantly to the fitness of an individual.

18
19 393 More data are needed: our conclusions are based on a total of 21 species.
20
21 394 However, the data collected to date are consistent with the hypothesis of maximum
22
23 395 packing, confirming Buller's drop radius is likely to be finely tuned to control range and
24
25 396 speed. How tuning evolves and the biomechanics underpinning ballistospory, a purely
26
27 397 extracellular process operating in the context of fluctuating environments, remains a
28
29 398 fascinating question for future research.

30
31
32
33
34
35 399

36 37 400 **ACKNOWLEDGEMENTS**

38
39
40 401 This work was supported by the Agence Nationale de la Recherche Investissements
41
42 402 d'Avenir UCA^{JEDI} #ANR-15-IDEX-01, by the Centre National de la Recherche
43
44 403 Scientifique Project international de cooperation scientifique (PICS) "2FORECAST",
45
46 404 by the Thomas Jefferson Fund a program of FACE and by the Global Health Institute at
47
48 405 the University of Wisconsin-Madison. Research at the Huron Mountains was supported
49
50 406 by the Huron Mountain Wildlife Foundation. We would like also to thank Sarah
51
52 407 Swanson for all her help and discussions about confocal microscopy.

53
54
55
56
57
58
59 408
60
61
62
63
64
65

1
2
3
4
5
6
7
8
9
10
11
12
13
14
15
16
17
18
19
20
21
22
23
24
25
26
27
28
29
30
31
32
33
34
35
36
37
38
39
40
41
42
43
44
45
46
47
48
49
50
51
52
53
54
55
56
57
58
59
60
61
62
63
64
65

409 **LITERATURE CITED**

- 410 Blackwell M. 2011. The fungi: 1,2,3, ... 5.1 million species? *American Journal of*
411 *Botany* 98:426–438.
- 412 Buller AHR. 1909. *Researches on Fungi*, Vol. II. London, U.K: Longmans, Green and
413 Co. 416 p.
- 414 de Gennes PJ. 1985. Wetting: statistics and dynamics. *Review of Modern Physics*
415 57:827–863.
- 416 Fischer MWF, Money NP. 2010. Why mushrooms form gills: efficiency of the
417 lamellate morphology. *Fungal Biology* 114:57–63.
- 418 Fischer MWF, Stolze-Rybczynski JL, Davis DJ, Cui Y, Money NP. 2010a. Solving the
419 aerodynamics of fungal flight: how air viscosity slows spore motion. *Fungal Biology*
420 114:943-948.
- 421 Fischer MW, Stolze-Rybczynski JL, Yunluan CUI, Money NP. 2010b. How far and
422 how fast can mushroom spores fly? Physical limits on ballistospore size and discharge
423 distance in the basidiomycota. *Fungal Biology* 114:669–675.
- 424 Fisher MC, Henk DA, Briggs CJ, Brownstein JS, Madoff LC, McCraw SL, Gurr SJ.
425 2012. Emerging fungal threats to animal, plant and ecosystem health. *Nature* 484:186–
426 194.
- 427 Hoorfar M, Kurz MA, Policova Z, Hair ML, Neumann AW. 2006. Do Polysaccharides
428 such as dextran and their monomers really increase the surface tension of water?
429 *Langmuir* 22:52–56.
- 430 Hussein T, Norros V, Hakala J, Petaja T, Aalto PP, Rannik U, Vesala T, Ovaskainen O.

1
2
3
4
5
6
7
8
9
10
11
12
13
14
15
16
17
18
19
20
21
22
23
24
25
26
27
28
29
30
31
32
33
34
35
36
37
38
39
40
41
42
43
44
45
46
47
48
49
50
51
52
53
54
55
56
57
58
59
60
61
62
63
64
65

431 2013. Species traits and inertial deposition of fungal spores. *Journal Aerosol Science*
432 61:81–98.

433 Liu F, Chavez RL, Patek SN, Pringle A, Feng JJ, Chen CH. 2017. Asymmetric drop
434 coalescence launches fungal ballistospores with directionality. *Journal of the Royal*
435 *Society Interface* 14:20170083.

436 McKnight KB, Roundy RO. 1991. Optimal gill packing in agaric sporocarps.
437 *Journal of Theoretical Biology* 150:497–528.

438 Kues U, Liu Y. 2000. Fruiting body production in basidiomycetes. *Applied Microbial*
439 *Biotechnology* 54:141–152.

440 Kupferschmidt K. 2012. Attack of the clones. *Science* 337:636–638.

441 Noblin X, Yang S, Dumais J. 2009. Surface tension propulsion of fungal spores. *The*
442 *Journal of Experimental Biology* 212:2835–2843.

443 Pennisi E. 2010. 1000 genomes project gives new map of genetic diversity. *Science*
444 329:574–575.

445 Phillips R. 1991. *Mushrooms of North America*. Boston, Massachusetts: Little, Brown
446 & Company. 319 p.

447 Pringle A, Patek S, Fischer M, Stolze J, Money N. 2005. The captured launch of a
448 ballistospore. *Mycologia* 97:866–871.

449 Schmitz J. 1843. *Beitrage zur Anatomie und Physiologie des Schwämme*. *Linnaea*
450 17:437.

451 Schoch CL, Seifert KA, Huhndorf S, Robert V, Spouge JL, Levesque CA, Chen W,

1
2
3
4
5
6
7
8
9
10
11
12
13
14
15
16
17
18
19
20
21
22
23
24
25
26
27
28
29
30
31
32
33
34
35
36
37
38
39
40
41
42
43
44
45
46
47
48
49
50
51
52
53
54
55
56
57
58
59
60
61
62
63
64
65

452 Fungal Barcoding Consortium. 2012. Nuclear ribosomal internal transcribed spacer
453 (ITS) region as a universal DNA barcode marker for Fungi. Proceedings of the National
454 Academy of Sciences, 109:6241–6246.

455 Stolze-Rybczynski JL. 2009. Biomechanics of spore discharge in the basidiomycota.
456 PhD Thesis, Oxford, Ohio: Miami University.

457 Stolze-Rybczynski JL, Cui Y, Henry M, Stevens H, Davis DJ, Fischer MW, Money NP.
458 2009. Adaptation of the spore discharge mechanism in the Basidiomycota. Plos One
459 4:e4163.

460 Stokes GG. 1951. On the effect of internal friction of fluids on the motion of
461 pendulums. Transactions of the Cambridge Philosophical Society 9:8–106.

462 Wang H, Qi M, Cutler AJ. 1993. A simple method of preparing plant samples for PCR.
463 Nucleic Acids Research 21:4153.

464 Webster J, Davey RA, Ingold CT. 1984. Ballistospore discharge in *Itersonilia*
465 *perplexans*. Transactions of the British Mycological Society. 82:13–29.

466 Webster J, Davey RA, Turner JCR. 1989. Vapour as the source of water in Buller’s
467 drop. Mycological Research 93:297–302.

468 Webster J, Davey RA, Smirnoff N, Fricke W, Hinde P, Tomos D, Turner JCR. 1995.
469 Mannitol and hexoses are components of Buller’s drop. Mycological Research 99:833–
470 838.
471

1
2
3
4
5
6
7
8
9
10
11
12
13
14
15
16
17
18
19
20
21
22
23
24
25
26
27
28
29
30
31
32
33
34
35
36
37
38
39
40
41
42
43
44
45
46
47
48
49
50
51
52
53
54
55
56
57
58
59
60
61
62
63
64
65

472 **FIGURE LEGENDS and FOOTNOTES**

473 **Figure 1.** Our current understanding of the surface tension catapult. Left to right:
474 Spore and structure holding spore; Buller's drop forms and grows by condensation
475 at the base of the spore (blue arrows). At the same time, the adaxial drop (visible
476 to some extent in the central frame, and indicated by blue arrows) grows on the
477 surface of the spore also by condensation (blue arrows). At a critical size, Buller's
478 drop collapses onto the adaxial drop and reduces the total liquid surface, thus
479 releasing energy. The released energy is converted into kinetic energy, catapulting
480 the spore away from its parent. The size of Buller's drop, together with material
481 parameters, determines the speed of spore discharge. Image adapted from
482 (Webster et al. 1984).

483
484 **Figure 2.** Collection and analysis of gill spacing in wild mushrooms. A. An image of
485 the underside of a mushroom cap collected fall 2017 in Michigan. B. Spore print
486 obtained by placing the spore cap on half aluminum foil/ half paper overnight. C.
487 Confocal microscope image of a sample of spores from the spore print. D. Segmentation
488 of image, used to recover spore contours. E. Concentric circles around the center of the
489 cap mark where intergill distances were measured and define the azimuthal angle θ ,
490 used to compute intergill distance. F. Gray scale values from image in E, as a function
491 of azimuthal angle θ . Peaks correspond to gills (white in the image of E), while troughs
492 correspond to the spaces between gills (dark or black in the image of E). To obtain
493 intergill distance, we marked all peaks (note arrows) and kept track of their azimuthal
494 angles. G. Close-up image showing locations of two peaks, marked by arrows 1 and 2.
495 Intergill distance $\Delta\theta$ is defined in radians, as the peak-to-peak distance (difference in
496 azimuthal angle of two adjacent peaks) minus the width of the gills themselves (width 1

1
2
3
4
5
6
7
8
9
10
11
12
13
14
15
16
17
18
19
20
21
22
23
24
25
26
27
28
29
30
31
32
33
34
35
36
37
38
39
40
41
42
43
44
45
46
47
48
49
50
51
52
53
54
55
56
57
58
59
60
61
62
63
64
65

497 and width 2 - see Materials and Methods). We calculated intergill distances in *mm* by
498 multiplying $\Delta\theta$ for the radius of the circle (r_c in panel E).

499 **Figure 3.** A. Energy balance from eq (1) predicts discharge speed. We represent the
500 normalized speed v_0/U as a function of y defined as the ratio of Buller's drop radius R_B
501 divided by spore radius R_s (red line). The thickness of the red line represents predicted
502 speed for β ranging from 1 to 2, where β is the ratio of spore to drop density. B. Linear
503 scaling between spore radius and Buller's drop radius from data published in the
504 literature (see TABLE 3). Spore radius is calculated as described in the main text.

505
506 **Figure 4.** Mushroom cap morphology and the maximum packing of spores. A. From
507 left to right: Representative mushroom; detail of gill arrangement indicating sporobolus
508 (trajectories of individual spores); magnified view of adjacent gills with basidia and
509 basidiospores. Sporobolus are represented in faint gray in the center panel and black
510 arrows in the right panel; adapted from Buller's drawing (Buller 1909). Maximum
511 packing implies that spores initially travel a distance $x = v_0\tau$ to reach the midpoint
512 between two facing gills separated by $d = 2v_0\tau$ with v_0 and τ given by equations (1)
513 and (2). B. Prediction for normalized Buller's drop radius at maximum packing, y_{pack} ,
514 obtained by numerically solving Equation (3) with the parameters listed in Table 1.
515 y_{pack} is color coded from 0 (cyan) to 4.4 (black); white corresponds to the value
516 $\langle y_{literature} \rangle = 32\%$. Symbols correspond to data of intergill distances and spore radii
517 measured from 8 species collected by us in Michigan and Wisconsin (see Figure 4).
518 Each symbol is linked with a species as in Figure 5, 6 and Table 2. The optimal Buller's
519 drop radius for the 8 collected species is $y_{pack} \sim 0.32 \pm 0.12$, where we report average
520 \pm standard deviation. The free parameters α and ρ_s are chosen within their range of
521 natural variation. The prediction varies little across the range of variation of α and ρ_s .

522

523 **Figure 5.** Spore size does not vary across a single mushroom cap. Gray thin lines mark
524 measurements of spore radius taken at three different distances from cap stipes with
525 errorbar representing standard deviation; means and standard deviations for spore radius
526 at all distances are shown in dark red vertical lines. Horizontal red line guides the eye.

527

528 **Figure 6.** Average gill spacing varies little with distance from cap stipes, a result driven
529 by the appearance of secondary gills at greater distances from the cap stipe. Gray lines
530 show all measures at various distances from the center, vertical red lines show the
531 average and standard deviation. Horizontal red line guides the eye. The only exception
532 is *Russula* sp. which has no secondary gills.

533 agnese.seminara@univ-cotedazur.fr

534

535

1
2
3
4
5
6
7
8
9
10
11
12
13
14
15
16
17
18
19
20
21
22
23
24
25
26
27
28
29
30
31
32
33
34
35
36
37
38
39
40
41
42
43
44
45
46
47
48
49
50
51
52
53
54
55
56
57
58
59
60
61
62
63
64
65

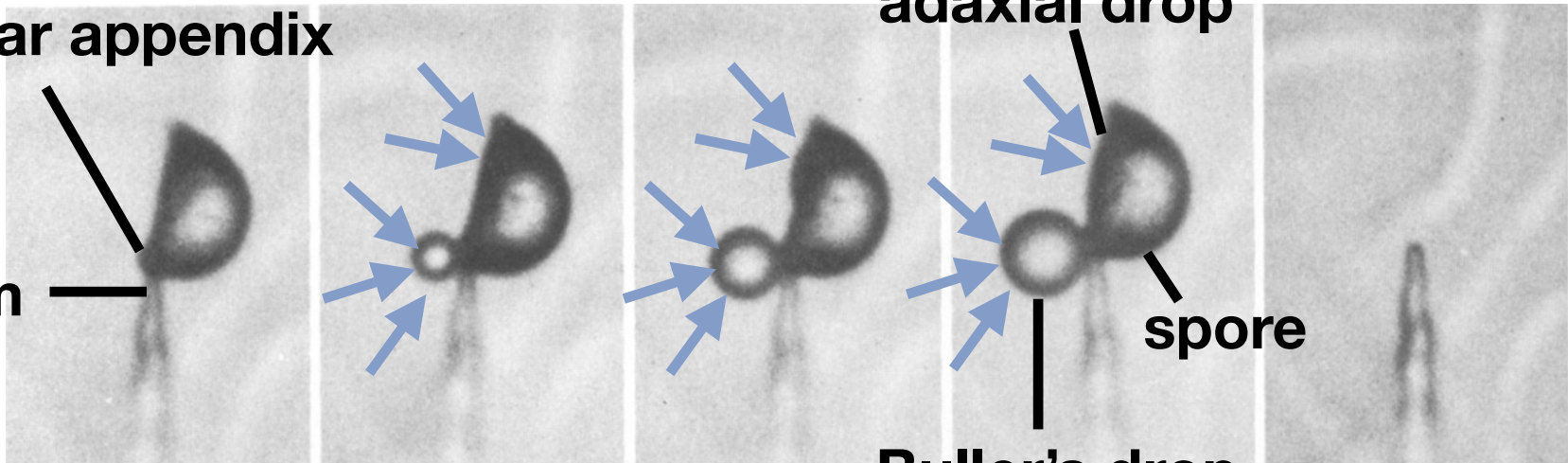
hilar appendix

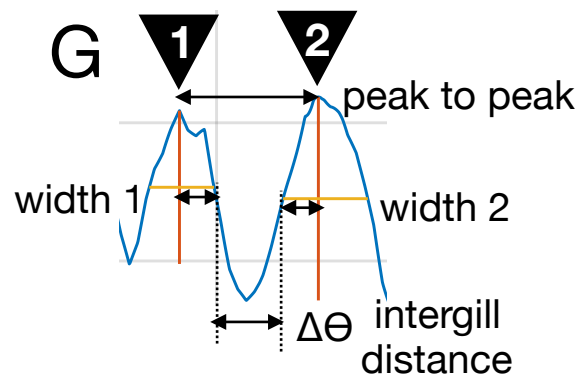
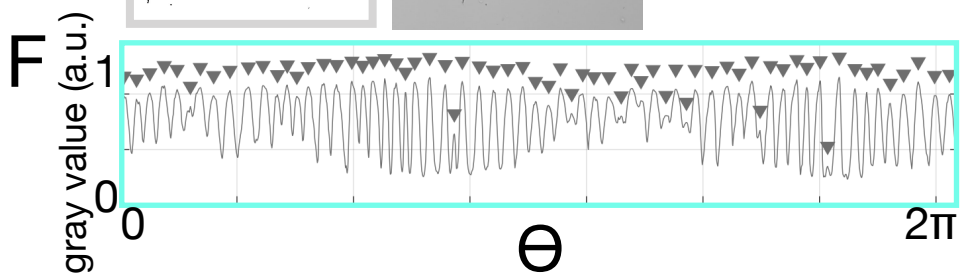
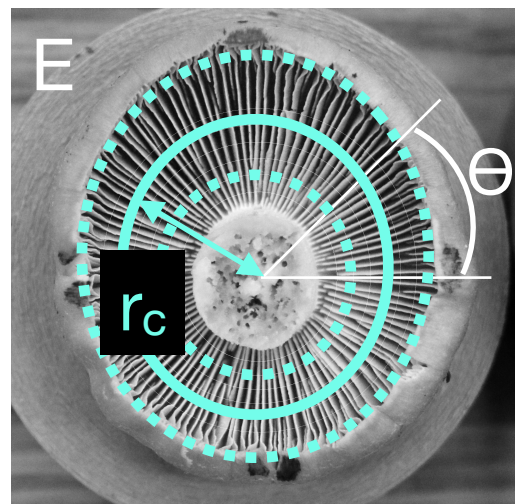
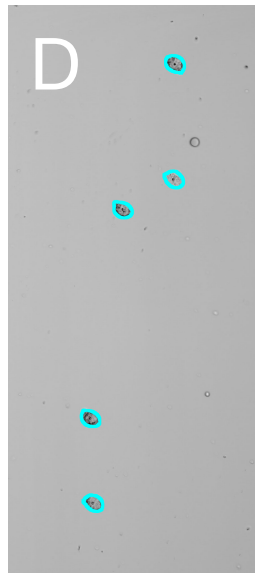
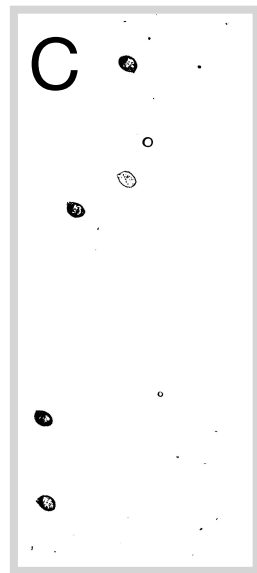
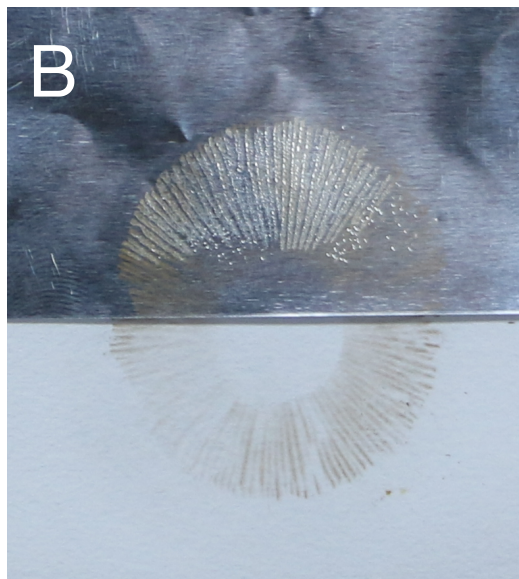
hilum

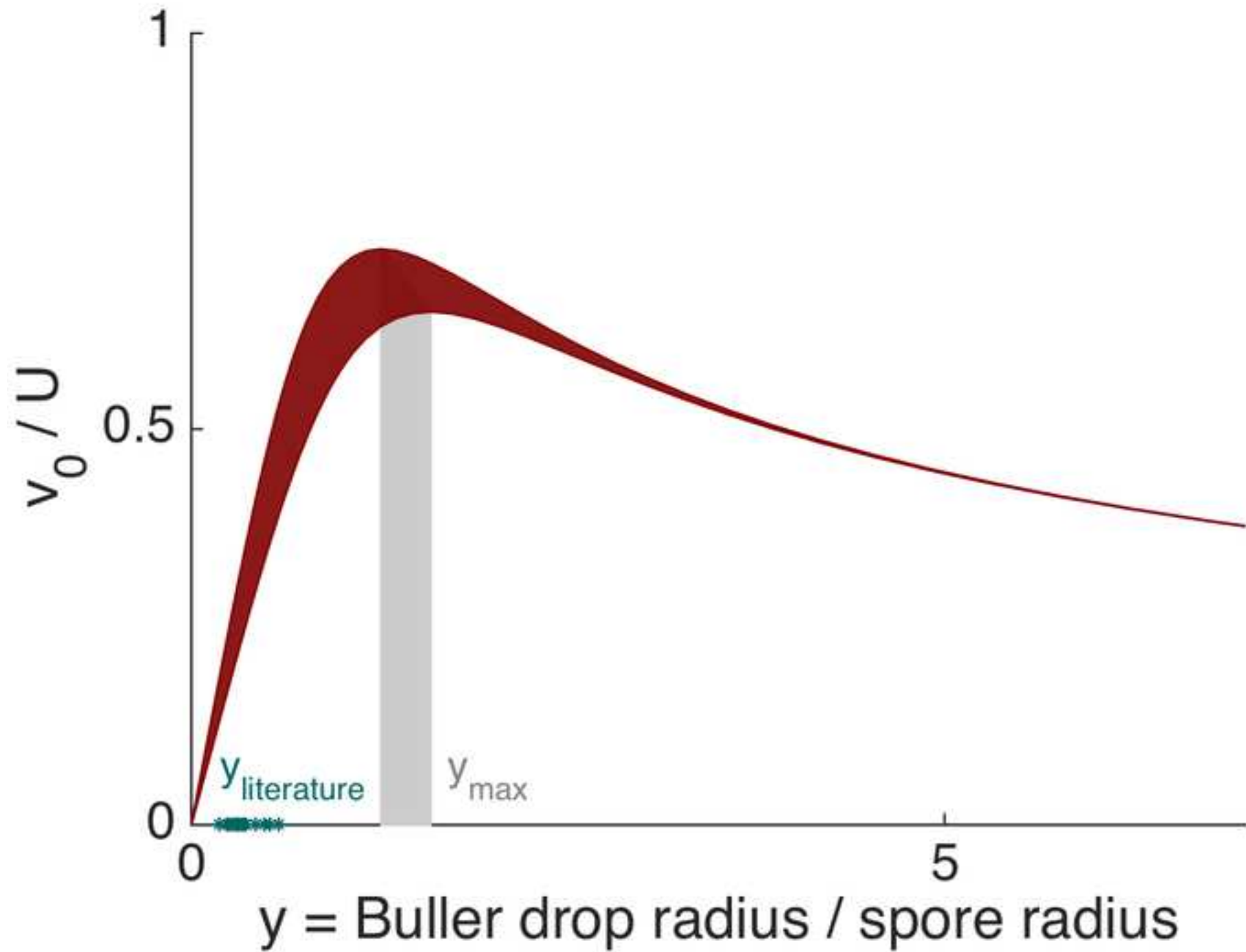
adaxial drop

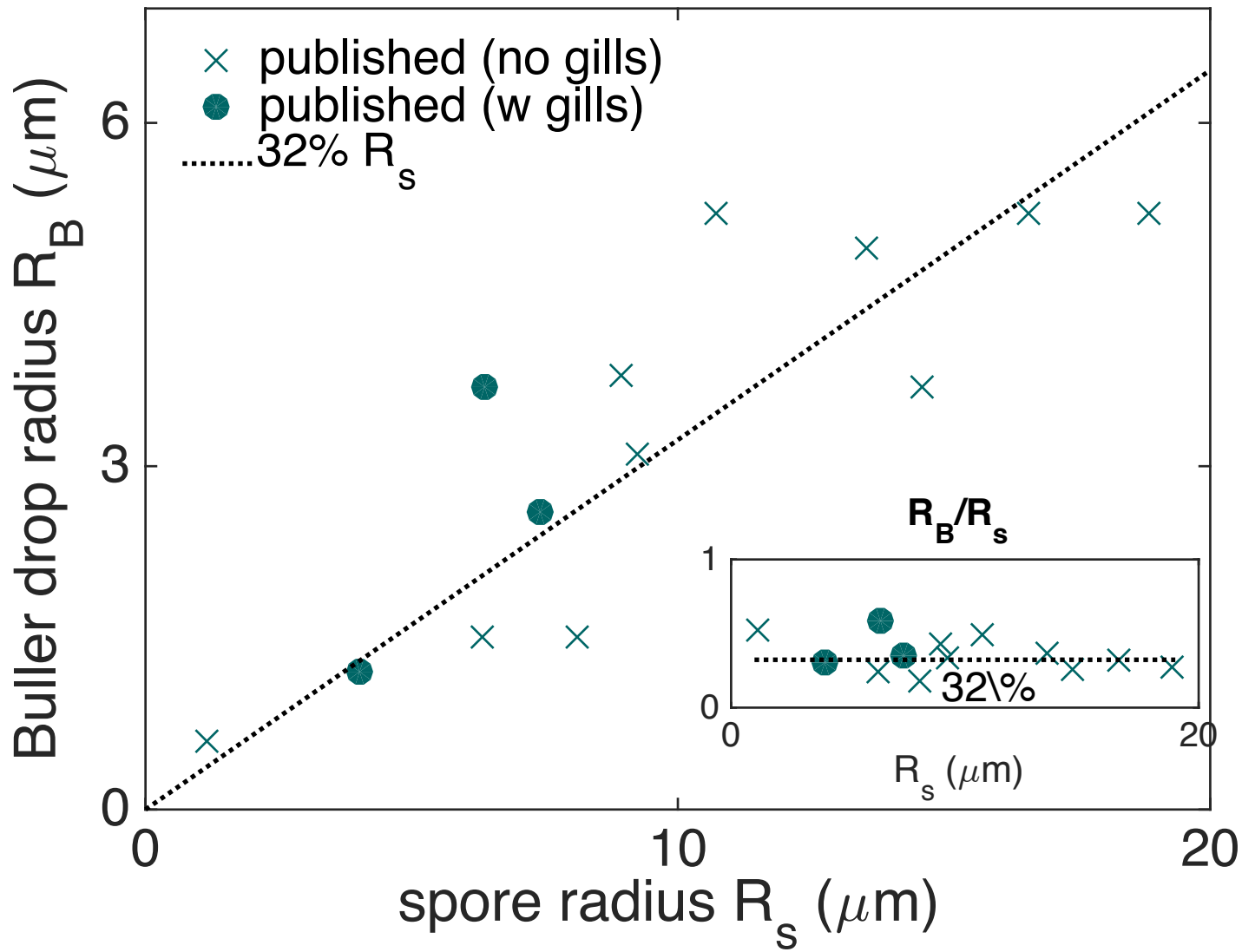
spore

Buller's drop

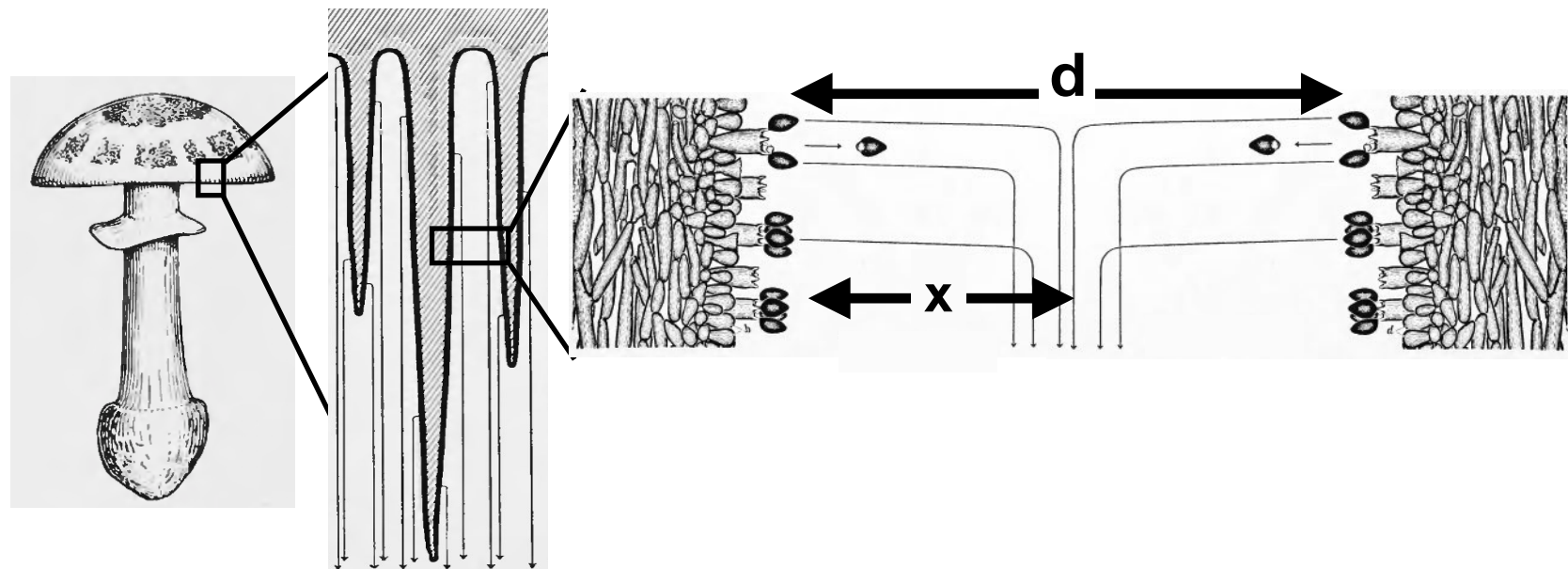






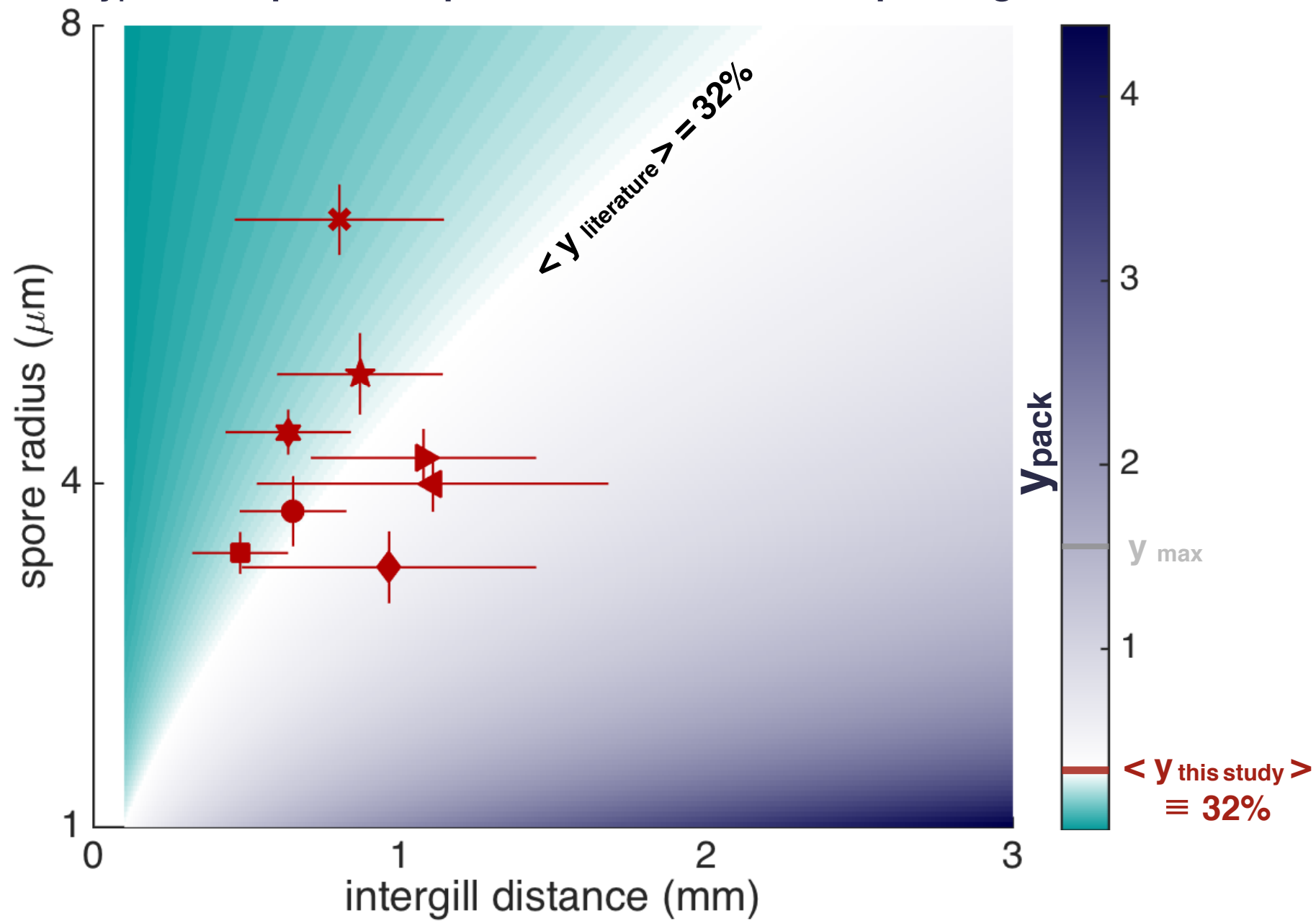


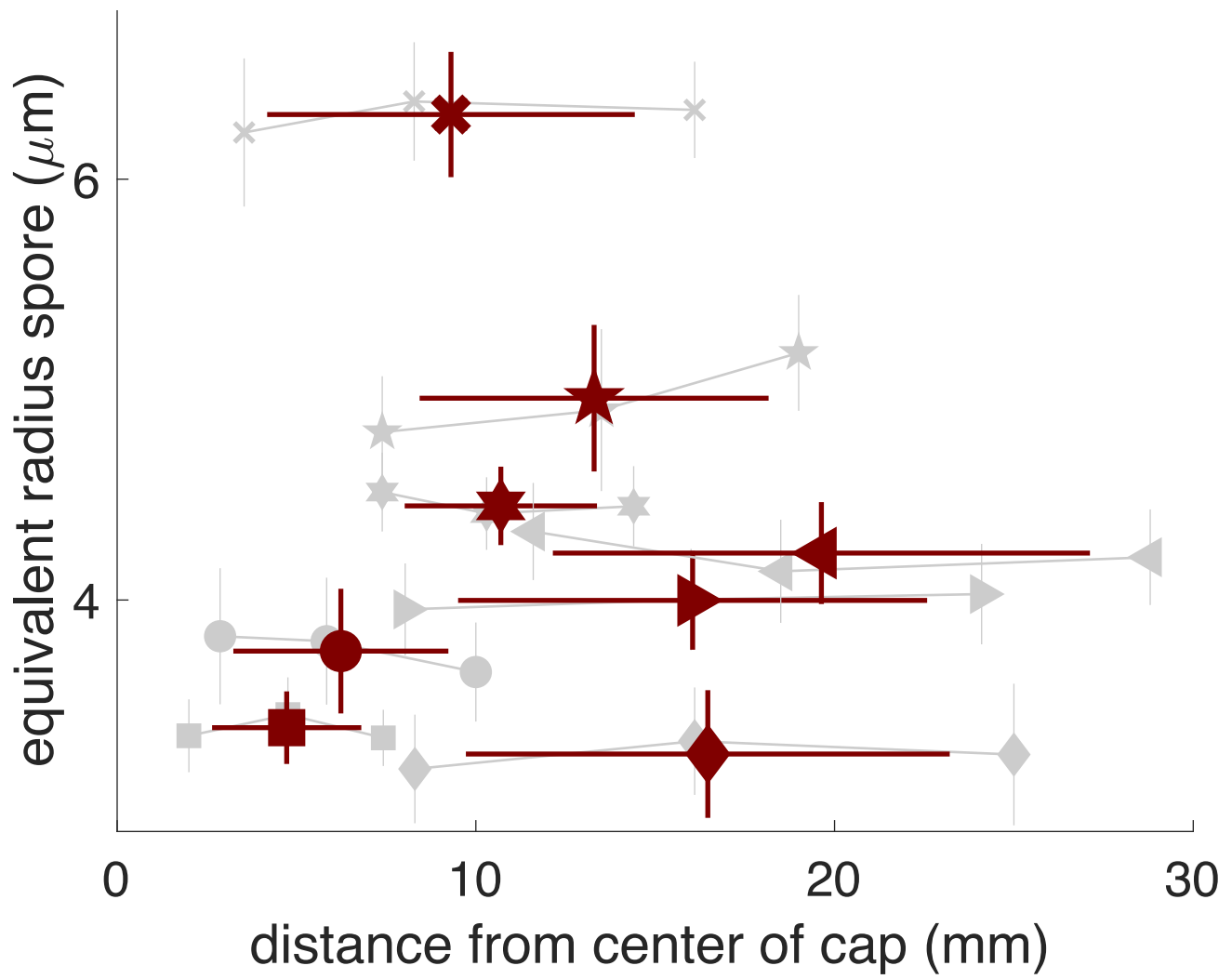
A



B

$y_{\text{pack}} = \text{drop radius/spore radius at maximum packing}$





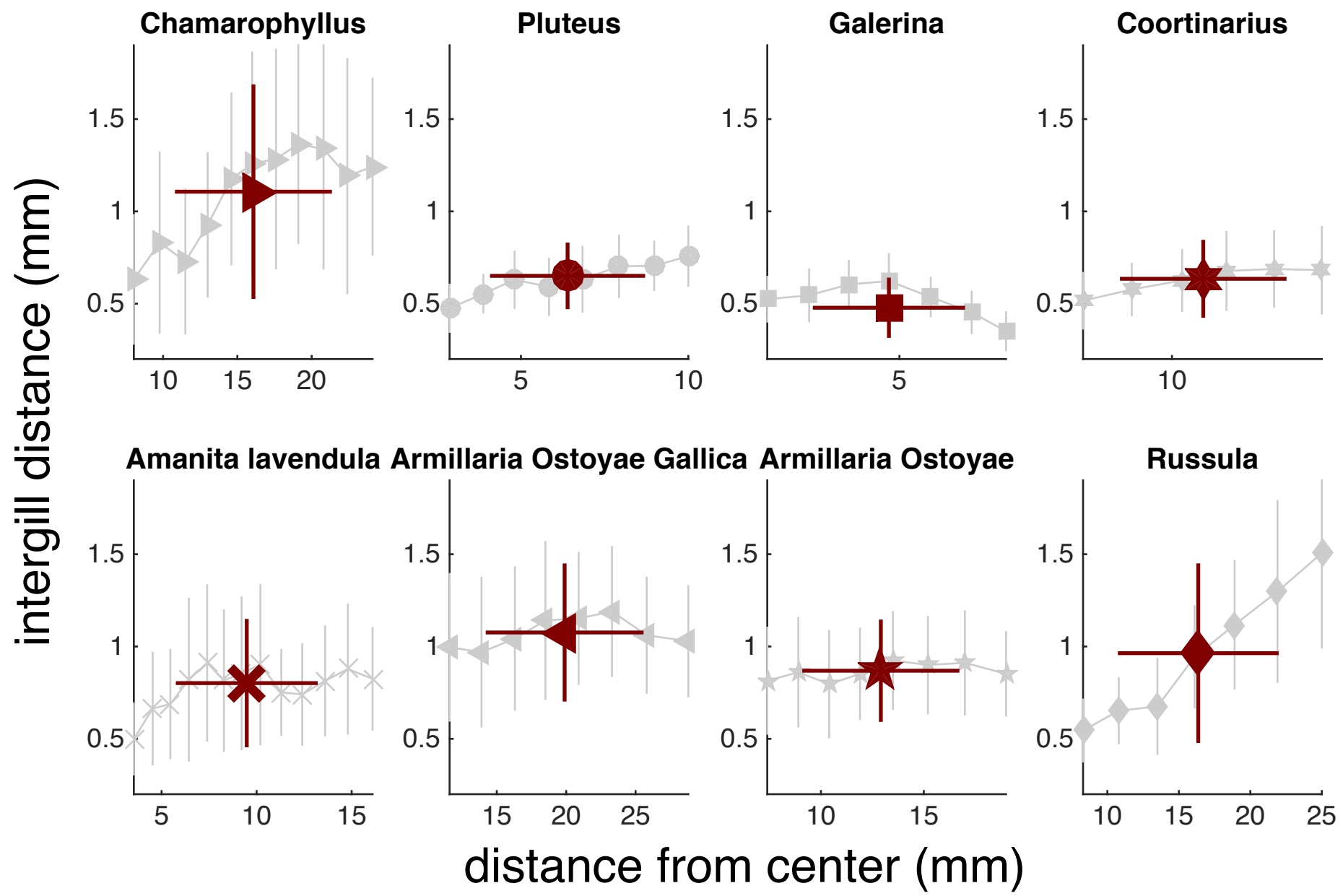


Table 1. List of parameters and their estimated or measured values from the literature.

Parameter	Symbol	Value	Reference	used in Fig 3
Air density	ρ_a	1 kg/m^3		1 kg/m^3
Spore density	ρ_s	0.8 to 3.8 g/m^3	(Hussein et al. 2013)	1.8 g/m^3
Buller's drop density	ρ_B	1 g/m^3	same as water ¹	1 g/cm^3
Buller's drop surface tension	γ	0.07 N/m	same as water ¹	0.07 N/m
Efficiency of energy conversion	α	$(50 \pm 5)\%$	(Noblin et al. 2009)	0.5
Spore to Buller's drop density ratio	$\beta = \rho_s/\rho_B$			
Air to Buller's drop density ratio	$\bar{\beta} = \rho_a/\rho_B$			
Reynolds number	$Re_B = R_s\gamma/(v^2\rho_B)$			
Reynolds number	$Re_s = R_s\gamma/(v^2\rho_s)$			
Intergill distance	d			
Spore radius	R_s			
Buller's drop radius	R_D			
Normalized Buller's drop radius	$y = R_B/R_s$			
y at maximum packing	y_{pack}			
Time scale	$T = 2R_s^2/(9v\bar{\beta})$			
Velocity scale				

¹Webster and coauthors estimated that Buller's drop contain about 1% in mass of mannitol and sucrose (Webster et al. 1995), hence γ and ρ_B are well approximated by the surface tension and density of water.

Table 2. List of collected species, collection location, number of spores imaged and analyzed, corresponding symbol used in Figures.

Collected species	Location	No. spores analyzed	Symbol
<i>Camarophyllus borealis</i>	Marquette County, Michigan	231	▶
<i>Cortinarius caperatus</i>	Marquette County, Michigan	1180	★
<i>Amanita lavendula</i>	Marquette County, Michigan	155	✕
<i>Armillaria mellea</i> complex (A)	Marquette County, Michigan	301	★
<i>Armillaria mellea</i> complex (B)	Marquette County, Michigan	257	◀
<i>Mycena</i> sp.	UW-Madison Lakeshore Natural Preserve, Wisconsin	530	●
<i>Russula</i> sp.	UW-Madison Lakeshore Natural Preserve, Wisconsin	1053	◆
<i>Galerina marginata</i>	UW-Madison Lakeshore Natural Preserve, Wisconsin	1159	■

Table 3. Data of Buller's drop radius and spore radius from the literature. From left to right: Name of species, structure bearing spores, Buller's drop radius R_B , spore length L_S , spore width W_S , spore volume V_S , spore equivalent radius R_S , reference; species that produce gilled mushrooms are in boldface.

Species (order or class)	Spore-bearing structure	R_B (μm)	L_S (μm)	W_S (μm)	V_S (μm)	R_S (μm)	Reference
<i>Trametes versicolor</i> (Polyporales)	Pores	0.6	-	-	6.4	1.15	Fischer et al. 2010
<i>Aleurodiscus oakesii</i> (Russulales)	Smooth, discoid	5.2	23.2	17.0	-	18.86	Pringle et al. 2010
<i>Itersonilia perplexans</i> (Tremellales)	Yeast	4.9	15.1	12.8	-	13.52	Pringle et al. 2010
<i>Tilletiopsis albescens</i> (Exobasidiomycetes, incertae sedis)	Yeast	3.7	13.4	4.4	-	6.38	Pringle et al. 2010
<i>Laccaria amethystina</i> (Agricales)	Gills	1.5	8.1	8.1	-	8.1	Stolze-Rybczynski 2009
<i>Stereum hirsutum</i> (Russulales)	Pores	1.2	7.2	3.0	-	4.02	Stolze-Rybczynski 2009
<i>Xerula radicata</i> (Agaricales)	Gills	3.7	16.8	13.6	-	14.59	Stolze-Rybczynski 2009
<i>Gymnosporangium juniperi-virginianae</i> (Pucciniales)	Gelatinous telial horns	5.2	20.0	15.1	-	16.58	Stolze-Rybczynski 2009
<i>Tilletia caries</i> (Tilletiales)	Host tissue	5.2	21.4	7.6	-	10.73	Stolze-Rybczynski 2009
<i>Sporobolomyces salmonicolor</i> (Sporidiobolales)	Yeast	3.8	11.5	7.9	-	8.95	Stolze-Rybczynski 2009
<i>Auricularia auricula</i> (Auriculariales)	Smooth, jelly-like	3.1	12.9	7.8	-	9.22	Stolze-Rybczynski 2009
<i>Polyporus squamosus</i> (Polyporales)	Pores	2.6	14.0	5.4	-	7.41	Stolze-Rybczynski 2009
<i>Armillaria tabescens</i> (Agaricales)	Gills	1.5	6.8	6.1	-	6.32	Stolze-Rybczynski 2009
<i>Clavicornia pyxidata</i> (Russulales)	Smooth, coral-like	1.2	4.7	3.5	-	3.86	Stolze-Rybczynski 2009